INTERNATIONAL JOURNAL FOR NUMERICAL METHODS IN FLUIDS
Int. J. Numer. Meth. Fluids 2003; **41**:3–27 (DOI: 10.1002/fld.375)

Numerical solution of steady free-surface flows by the adjoint optimal shape design method

E. H. van Brummelen[1,*,†] and A. Segal[2]

[1] *CWI, P.O. Box 94079, 1090 GB Amsterdam, The Netherlands*
[2] *Delft University of Technology, P.O. Box 5031, 2600 GA Delft, The Netherlands*

SUMMARY

Numerical solution of flows that are partially bounded by a freely moving boundary is of great importance in practical applications such as ship hydrodynamics. Free-boundary problems can be reformulated into optimal shape design problems, which can in principle be solved efficiently by the adjoint method. In this work we investigate the suitability of the adjoint shape optimization method for solving steady free-surface flows. The asymptotic convergence behaviour of the method is determined for free-surface flows in 2D and 3D. It is shown that the convergence behaviour depends sensitively on the occurrence of critical modes. The convergence behaviour is moreover shown to be mesh-width independent, provided that proper preconditioning is applied. Numerical results are presented for 2D flow over an obstacle in a channel. The observed convergence behaviour is indeed mesh-width independent and conform the derived asymptotic estimates. Copyright © 2003 John Wiley & Sons, Ltd.

KEY WORDS: numerical solution methods; steady free-surface flows; optimal shape design; adjoint methods

1. INTRODUCTION

The numerical solution of flows which are partially bounded by a freely moving boundary is of great importance in many engineering applications, e.g. ship hydrodynamics [1–3], hydraulics and coating technology [4, 5]. A practically relevant class of free-surface flow problems are *steady* free-surface flows. An example of such a steady free-surface flow is the wave pattern carried by a ship at forward speed in still water. The numerical techniques for free-surface potential flow are well developed; for an overview, see Reference [6]. In particular, dedicated techniques have been developed for solving the steady free-surface potential-flow equations, e.g. Reference [7]. In contrast, methods for the steady free-surface Navier–Stokes equations typically continue a transient process until a steady state is reached. This time-integration method is often computationally inefficient, due to the specific transient behaviour of

* Correspondence to: Harald van Brummelen, CWI, P.O. Box 94079, 1090 GB Amsterdam, The Netherlands.
† E-mail: e.h.vanbrummelen@lr.tudelft.nl

Contract/grant sponsor: Maritime Research Institute Netherlands.

free-surface flows; see References [8, 9]. Alternative solution methods for the steady free-surface Navier–Stokes equations exist. However, the performance of these methods usually depends sensitively on the parameters in the problem, or their applicability is too restricted; see, for instance, References [4, 10]. In Reference [8], an efficient iterative algorithm was presented. However, the implementation of the quasi-free-surface condition that underlies the efficiency of this method can be involved. Hence, the investigation of numerical methods for the steady free-surface Navier–Stokes equations is warranted.

A general characteristic of free-boundary problems is that the number of free-boundary conditions is one more than the number of boundary conditions required by the governing boundary value problem. A free-boundary problem can therefore be reformulated into the equivalent shape optimization problem of finding the boundary that minimizes a norm of the residual of one of the free-surface conditions, subject to the boundary value problem with the remaining free-surface conditions imposed.

Optimal shape design problems can in principle be solved efficiently by means of the adjoint method. In recent years, much progress has been made in the development of adjoint techniques for problems from fluid dynamics. Applications to the Navier–Stokes equations include flow control (see Reference [11] and the references therein), *a posteriori* error-estimation and adaptivity (for instance, Reference [12]), optimal design (e.g. References [13, 14]) and domain decomposition (cf. Reference [15]). The techniques that are required to solve the optimal shape design problem associated with steady free-surface flow are readily available.

The present work investigates the suitability of the adjoint shape optimization method for solving steady free-surface flow problems. Our primary interest is in the steady free-surface Navier–Stokes equations. However, because inviscid, irrotational flow adequately describes the prominent features of free-surface flow and to avoid the excessive complexity of the Navier–Stokes equations, we base our investigation on the free-surface potential-flow equations. It is anticipated that the adjoint shape optimization method is equally applicable to the free-surface Navier–Stokes equations, although the specifics of the method are much more involved in that case. Our investigation serves as an indication of the properties of the adjoint shape optimization method for steady free-surface flow problems.

The contents of the paper are organized as follows: In Section 2 the equations governing steady free-surface potential flow and the associated design problem are stated. Section 3 formulates the adjoint equations and sets up the adjoint optimization method. Section 4 presents an analysis of the properties of the optimization problem and the convergence behaviour of the adjoint method, using Fourier techniques from Reference [16]. Motivated by the results of the Fourier analysis, we describe a preconditioning for the optimization problem in Section 5. Numerical experiments and results are presented in Section 6. Section 7 contains concluding remarks.

2. PROBLEM STATEMENT

We consider an incompressible, inviscid fluid flow, subject to a constant gravitational force, acting in the negative vertical direction. The fluid occupies a domain $\mathscr{V} \subset \mathbb{R}^d$ $(d = 2, 3)$ which is bounded by a free boundary, $\mathscr{S}$, and a fixed boundary $\partial\mathscr{V} \setminus \mathscr{S}$. The fixed boundary can be subdivided in an inflow boundary, an outflow boundary and a rigid, impermeable boundary.

2.1. Governing equations

The (non-dimensionalized) fluid velocity and pressure are identified by $\mathbf{v}(\mathbf{x})$ and $p(\mathbf{x})$, respectively. Assuming that the velocity-field is irrotational, a velocity-potential $\phi(\mathbf{x})$ exists such that $\mathbf{v} = \nabla\phi$. Enforcing incompressibility then yields that the velocity-potential is governed by Laplace's equation,

$$\Delta\phi = 0, \quad \mathbf{x} \in \mathscr{V} \tag{1}$$

Assuming that $|\nabla\phi| = 1$ at the inflow boundary, Bernoulli's equation relates the pressure to the velocity-potential by

$$p(\mathbf{x}) = \tfrac{1}{2} - (\tfrac{1}{2}|\nabla\phi|^2 + \mathrm{Fr}^{-2}x_d) \tag{2}$$

with x_d the vertical co-ordinate and Fr the Froude number, defined by $\mathrm{Fr} \equiv V/\sqrt{gL}$ with V an appropriate reference velocity, g the gravitational acceleration and L a reference length.

The free-surface conditions prescribe that the free surface is impermeable and that the pressure vanishes at the free surface:

$$\mathbf{n} \cdot \nabla\phi = 0, \quad \mathbf{x} \in \mathscr{S} \tag{3a}$$

$$p = 0, \quad \mathbf{x} \in \mathscr{S} \tag{3b}$$

with $\mathbf{n}(\mathbf{x})$ the unit normal vector to $\mathscr{S}$. Conditions (3a) and (3b) are referred to as the kinematic condition and the dynamic condition, respectively. A single appropriate boundary condition must be specified at the fixed boundary. We assume that this condition is of the form

$$a\mathbf{n} \cdot \nabla\phi + b\phi = c, \quad \mathbf{x} \in \partial\mathscr{V} \backslash \mathscr{S} \tag{4}$$

for certain functions $a, b, c : \partial\mathscr{V} \backslash \mathscr{S} \mapsto \mathbb{R}$.

The steady free-surface flow problem under consideration is the problem of finding $\mathscr{S}$ and ϕ such that ϕ satisfies (1)–(4). However, this problem is not necessarily well-posed. Firstly, solutions can be non-unique due to the occurrence of arbitrary non-physical upstream waves. To remove these waves, a radiation condition must be imposed; cf., for instance, References [17–19]. In numerical computations, this radiation condition can be conveniently enforced by introducing artificial damping (see Section 6) or by selecting a suitable discretization (see, e.g. Reference [7]). Secondly, a steady solution can be non-existent, in the sense that the transient problem underlying (1)–(4) does not approach a steady state as time progresses *ad infinitum*; see, for instance, Reference [9].

2.2. Optimal shape design formulation

One may note that the number of free-surface conditions (3) is one more than the number of boundary conditions required by (1). The free-boundary problem can therefore be reformulated into the equivalent optimal-shape design problem of finding the boundary that minimizes a norm of the residual of one of the free-surface conditions, subject to the boundary value problem with the remaining free-surface conditions imposed.

To obtain an optimal-shape design formulation of the steady free-surface flow problem, the *cost functional* E is defined by

$$E(\mathscr{S},\phi)=\int_{\mathscr{S}}\tfrac{1}{2}\,p(\mathbf{x})^2\,\mathrm{d}\mathbf{x} \tag{5}$$

and the *constraint* C is defined by the boundary value problem (1), (3a) and (4):

$$C(\mathscr{S},\phi)=\begin{cases}\Delta\phi=0, & \mathbf{x}\in\mathscr{V}\\ \mathbf{n}\cdot\nabla\phi=0, & \mathbf{x}\in\mathscr{S}\\ a\,\mathbf{n}\cdot\nabla\phi+b\phi=c, & \mathbf{x}\in\partial\mathscr{V}\setminus\mathscr{S}\end{cases} \tag{6}$$

Note that the cost functional is a norm of the residual of the dynamic condition (3b) and that the kinematic condition (3a) appears in the constraint. The free-surface flow problem is equivalent to the optimal shape design problem

$$\min_{\mathscr{S}}\{E(\mathscr{S},\phi):C(\mathscr{S},\phi)\} \tag{7}$$

i.e. minimize (5) over all $\mathscr{S}$, subject to the constraint that ϕ satisfies (6). Because the boundary value problem (6) associates a unique ϕ with each free boundary $\mathscr{S}$, it is often convenient to use the notation $E(\mathscr{S})$ for $E(\mathscr{S},\phi)$ with ϕ from (6).

3. ADJOINT OPTIMIZATION METHOD

Shape-optimization problems can in principle be solved efficiently by means of the adjoint optimization method. The essential problem in treating shape-optimization problems is that a displacement of the free boundary induces a disturbance in the solution of the boundary value problem and, consequently, it is attended with an induced change in the cost functional. Efficient solution of a shape-optimization problem requires control over the induced change in the cost functional. The adjoint optimization method eliminates the induced change by means of the solution of a dual problem. Upon elimination of the induced change, the gradient of the cost functional with respect to the free-boundary position is obtained. Improvement of the free-boundary position is then straightforward. This section outlines the adjoint optimization method for solving (7).

3.1. Induced disturbance

To formulate the adjoint optimization method for (7), the induced disturbance in the solution of the constraint and the corresponding change in the cost functional must first be identified. To this end, we consider a domain $\mathscr{V}$ with free boundary $\mathscr{S}$ and a modified domain $\mathscr{V}_{\varepsilon\alpha}$ with free boundary

$$\mathscr{S}_{\varepsilon\alpha}=\{\mathbf{x}+\varepsilon\alpha(\mathbf{x})\mathbf{n}(\mathbf{x}):\ \mathbf{x}\in\mathscr{S}\} \tag{8}$$

where α is a smooth function on $\mathscr{S}$, independent of ε. Following [20], $\mathscr{V}$ and $\mathscr{V}_{\varepsilon\alpha}$ are embedded in a bounded set $\mathscr{E}$ and it is assumed that a solution of the constraint can be extended smoothly beyond the boundary, so that it is well defined in $\mathscr{E}$. Denoting by ϕ the solution of $C(\mathscr{S},\phi)$

and by $\phi_{\varepsilon\alpha}$ the solution of $C(\mathscr{S}_{\varepsilon\alpha}, \phi_{\varepsilon\alpha})$, we define the *induced disturbance* by the function $\phi'_\alpha : \mathscr{E} \mapsto \mathbb{R}$ with the property

$$\phi_{\varepsilon\alpha} = \phi + \varepsilon\phi'_\alpha + O(\varepsilon^2), \quad \text{as } \varepsilon \to 0 \tag{9}$$

i.e. $\varepsilon\phi'_\alpha$ approximates to $O(\varepsilon^2)$ the change in the solution of the constraint (6) due to the displacement of the free boundary from $\mathscr{S}$ to $\mathscr{S}_{\varepsilon\alpha}$. The kinematic condition corresponding to the modified boundary yields:

$$\begin{aligned}
&[\mathbf{n}_{\varepsilon\alpha} \cdot \nabla\phi_{\varepsilon\alpha}](\mathbf{x} + \varepsilon\alpha(\mathbf{x})\mathbf{n}(\mathbf{x})) \\
&\quad = \left[\left(\mathbf{n} - \varepsilon \sum_{j=1}^{d-1} (\mathbf{t}_j \cdot \nabla\alpha)\mathbf{t}_j + O(\varepsilon^2) \right) \cdot (\nabla\phi + \varepsilon\nabla\phi'_\alpha + \varepsilon\alpha\mathbf{n} \cdot \nabla\nabla\phi + O(\varepsilon^2)) \right](\mathbf{x}) \\
&\quad = 0, \quad \mathbf{x} \in \mathscr{S}
\end{aligned} \tag{10}$$

with $\mathbf{n}_{\varepsilon\alpha}$ the unit normal vector to $\mathscr{S}_{\varepsilon\alpha}$ and $\mathbf{t}_j$ orthogonal tangent vectors to $\mathscr{S}$. Hence, inserting (9) in $C(\mathscr{S}_{\varepsilon\alpha}, \phi_{\varepsilon\alpha})$ and collecting terms $O(\varepsilon)$, it follows that the induced disturbance satisfies the boundary value problem:

$$\Delta\phi'_\alpha = 0, \quad \mathbf{x} \in \mathscr{V} \tag{11a}$$

$$\mathbf{n} \cdot \nabla\phi'_\alpha = -\alpha\mathbf{n}\mathbf{n} : \nabla\nabla\phi + \sum_{j=1}^{d-1} (\mathbf{t}_j \cdot \nabla\alpha)(\mathbf{t}_j \cdot \nabla\phi), \quad \mathbf{x} \in \mathscr{S} \tag{11b}$$

$$a\mathbf{n} \cdot \nabla\phi'_\alpha + b\phi'_\alpha = 0, \quad \mathbf{x} \in \partial\mathscr{V} \setminus \mathscr{S} \tag{11c}$$

To identify the induced change in the cost functional, the functional value corresponding to the modified boundary, $E(\mathscr{S}_{\varepsilon\alpha})$, is expanded as

$$E(\mathscr{S}_{\varepsilon\alpha}) \equiv E(\mathscr{S}_{\varepsilon\alpha}, \phi_{\varepsilon\alpha}) = E(\mathscr{S}) + \varepsilon(I'_\alpha(\mathscr{S}) + J'_\alpha(\mathscr{S})) + O(\varepsilon^2), \quad \text{as } \varepsilon \to 0 \tag{12a}$$

with

$$I'_\alpha(\mathscr{S}) = -\int_{\mathscr{S}} p\,\nabla\phi \cdot \nabla\phi'_\alpha \mathrm{d}\mathbf{x} \tag{12b}$$

$$J'_\alpha(\mathscr{S}) = -\int_{\mathscr{S}} \alpha \left(\frac{p^2}{2R} + p\,\mathbf{n} \cdot \nabla\tfrac{1}{2}|\nabla\phi|^2 + p\,\mathrm{Fr}^{-2}\mathbf{n} \cdot \mathbf{e}_d \right) \mathrm{d}\mathbf{x} \tag{12c}$$

where $R(\mathbf{x})$ is the radius of curvature ($d=2$) or mean radius of curvature ($d=3$) and $\mathbf{e}_d$ is the vertical unit vector. The curvature-term in (12c) results from the change in the surface area from $\mathscr{S}$ to $\mathscr{S}_{\varepsilon\alpha}$; see, e.g. Reference [20]. Noting that only (12b) depends on ϕ'_α, the induced change in the cost functional is readily identified as (12b). Integration by parts recasts (12b)

into the convenient form:

$$I'_\alpha(\mathscr{S}) = \int_{\mathscr{S}} \phi'_\alpha \sum_{j=1}^{d-1} \mathbf{t}_j \cdot \boldsymbol{\nabla}(p\,\mathbf{t}_j \cdot \boldsymbol{\nabla}\phi)\,\mathrm{d}\mathbf{x} \tag{13a}$$

Moreover, the second term in (12c) vanishes due to the kinematic condition (3a):

$$J'_\alpha(\mathscr{S}) = -\int_{\mathscr{S}} \alpha\left(\frac{p^2}{2R} + p\,\mathrm{Fr}^{-2}\mathbf{n}\cdot\mathbf{e}_d\right)\mathrm{d}\mathbf{x} \tag{13b}$$

If $\alpha(\mathbf{x})$ is chosen such that $I'_\alpha + J'_\alpha < 0$, an adjustment of the free boundary from $\mathscr{S}$ to $\mathscr{S}_{\gamma\alpha}$, with γ a small positive number, results in a reduction of the cost functional and thus improves the approximation to the actual free-boundary position. Such a choice of α is called a *descent direction*.

3.2. Adjoint operators and duality

The inherent problem in determining a descent direction from (13), is the dependence of (13a) on ϕ'_α, which is connected to α through the boundary value problem (11). Equations (11) and (13) are useful to verify if a particular α is a descent direction. However, they are inept to determine a descent direction.

The adjoint optimization method uses the equivalence of (11), (13a) to its dual problem to eliminate the induced change in the functional. To define the duality property, adjoint operators must be introduced. Let $(\cdot,\cdot)_{\mathscr{V}}$ and $(\cdot,\cdot)_{\partial\mathscr{V}}$ denote the L_2 integral inner products over the domain $\mathscr{V}$ and its boundary $\partial\mathscr{V}$, respectively. Consider the linear boundary value problem:

$$L_i(\phi) = l_i, \quad \mathbf{x}\in\mathscr{V} \tag{14a}$$
$$L_b(\phi) = l_b, \quad \mathbf{x}\in\partial\mathscr{V} \tag{14b}$$

and the functional

$$I = (f_i, F_i(\phi))_{\mathscr{V}} + (f_b, F_b(\phi))_{\partial\mathscr{V}} \tag{15}$$

for certain interior operators L_i, F_i and boundary operators L_b, F_b. The adjoint operators L_i^*, F_i^* and adjoint boundary operators L_b^*, F_b^* are defined by the identity

$$(L_i^*(\lambda), F_i(\phi))_{\mathscr{V}} + (L_b^*(\lambda), F_b(\phi))_{\partial\mathscr{V}} = (F_i^*(\lambda), L_i(\phi))_{\mathscr{V}} + (F_b^*(\lambda), L_b(\phi))_{\partial\mathscr{V}} \tag{16}$$

for all appropriate functions ϕ and λ. For example, if

$$L_i(\phi) = \Delta\phi, \quad L_b(\phi) = a\mathbf{n}\cdot\boldsymbol{\nabla}\phi + b\phi, \quad F_i(\phi) = \phi, \quad F_b(\phi) = \underline{a}\mathbf{n}\cdot\boldsymbol{\nabla}\phi + \underline{b}\phi \tag{17a}$$

for certain functions $a, b, \underline{a}, \underline{b} : \partial\mathscr{V} \mapsto \mathbb{R}$ such that $b\underline{a} - a\underline{b} \neq 0$, then

$$L_i^*(\lambda) = L_i(\lambda), \quad L_b^*(\lambda) = \frac{L_b(\lambda)}{b\underline{a} - a\underline{b}}, \quad F_i^*(\lambda) = F_i(\lambda), \quad F_b^*(\lambda) = \frac{F_b(\lambda)}{b\underline{a} - a\underline{b}} \tag{17b}$$

To prove that (17a) and (17b) indeed satisfy the identity (16):

$$
\begin{aligned}
&(L_i^*(\lambda), F_i(\phi))_{\mathscr{V}} + (L_b^*(\lambda), F_b(\phi))_{\partial\mathscr{V}} \\
&\quad = \int_{\mathscr{V}} \phi\, \Delta\lambda \, \mathrm{d}\mathbf{x} + \oint_{\partial\mathscr{V}} \left(\frac{a\mathbf{n}\cdot\nabla\lambda + b\lambda}{b\underline{a} - a\underline{b}} \right) (\underline{a}\mathbf{n}\cdot\nabla\phi + \underline{b}\phi)\, \mathrm{d}\mathbf{x} \\
&\quad = \int_{\mathscr{V}} \lambda\, \Delta\phi \, \mathrm{d}\mathbf{x} + \oint_{\partial\mathscr{V}} (\phi\, \mathbf{n}\cdot\nabla\lambda - \lambda\, \mathbf{n}\cdot\nabla\phi)\, \mathrm{d}\mathbf{x} + \oint_{\partial\mathscr{V}} \left(\frac{a\mathbf{n}\cdot\nabla\lambda + b\lambda}{b\underline{a} - a\underline{b}} \right) (\underline{a}\mathbf{n}\cdot\nabla\phi + \underline{b}\phi)\, \mathrm{d}\mathbf{x} \\
&\quad = \int_{\mathscr{V}} \lambda\, \Delta\phi \, \mathrm{d}\mathbf{x} + \oint_{\partial\mathscr{V}} \left(\frac{\underline{a}\mathbf{n}\cdot\nabla\lambda + \underline{b}\lambda}{b\underline{a} - a\underline{b}} \right) (a\mathbf{n}\cdot\nabla\phi + b\phi)\, \mathrm{d}\mathbf{x} \\
&\quad = (F_i^*(\lambda), L_i(\phi))_{\mathscr{V}} + (F_b^*(\lambda), L_b(\phi))_{\partial\mathscr{V}}
\end{aligned}
$$

From the identity (16) it follows that (15) subject to (14) is equivalent to

$$I = (l_i, F_i^*(\lambda))_{\mathscr{V}} + (l_b, F_b^*(\lambda))_{\partial\mathscr{V}} \tag{18}$$

subject to

$$L_i^*(\lambda) = f_i, \quad \mathbf{x} \in \mathscr{V} \tag{19a}$$

$$L_b^*(\lambda) = f_b, \quad \mathbf{x} \in \partial\mathscr{V} \tag{19b}$$

To prove the equivalence:

$$
\begin{aligned}
I = (f_i, F_i(\phi))_{\mathscr{V}} + (f_b, F_b(\phi))_{\partial\mathscr{V}} &= (L_i^*(\lambda), F_i(\phi))_{\mathscr{V}} + (L_b^*(\lambda), F_b(\phi))_{\partial\mathscr{V}} \\
&= (F_i^*(\lambda), L_i(\phi))_{\mathscr{V}} + (F_b^*(\lambda), L_b(\phi))_{\partial\mathscr{V}} \\
&= (F_i^*(\lambda), l_i)_{\mathscr{V}} + (F_b^*(\lambda), l_b)_{\partial\mathscr{V}}
\end{aligned} \tag{20}
$$

In this context, (14)–(15) is called the primal problem and (18)–(19) is called the dual problem. Duality is the equivalence of the primal and dual problem.

The adjoint optimization method uses duality to eliminate the induced change in the cost functional (13a). Observe that for given ϕ, the functional (13a) is the L_2 inner product of ϕ'_α with a given function and (11) acts as a constraint on ϕ'_α. Hence, (13a) subject to (11) is of the form (14)–(15). To obtain the dual problem for (11)–(13a), we note that (11) implies

$$
\begin{aligned}
&\int_{\mathscr{V}} \lambda \Delta\phi'_\alpha \mathrm{d}\mathbf{x} + \int_{\mathscr{S}} \psi\, \mathbf{n}\cdot\nabla\phi'_\alpha \, \mathrm{d}\mathbf{x} + \int_{\mathscr{S}} \psi \left(\alpha\, \mathbf{nn} : \nabla\nabla\phi - \sum_{j=1}^{d-1} (\mathbf{t}_j\cdot\nabla\alpha)(\mathbf{t}_j\cdot\nabla\phi) \right) \mathrm{d}\mathbf{x} \\
&\quad + \int_{\partial\mathscr{V}\setminus\mathscr{S}} \psi\, (a\, \mathbf{n}\cdot\nabla\phi'_\alpha + b\phi'_\alpha)\, \mathrm{d}\mathbf{x} = 0
\end{aligned} \tag{21}
$$

for all admissible functions $\lambda : \mathscr{V} \mapsto \mathbb{R}$ and $\psi : \partial\mathscr{V} \mapsto \mathbb{R}$. The operator $\mathbf{nn} : \boldsymbol{\nabla}\boldsymbol{\nabla}$ in (21) represents the second derivative in the normal direction. Integrating by parts, (21) can be recast into

$$\int_{\mathscr{V}} \phi'_\alpha \Delta\lambda \, \mathrm{d}\mathbf{x} - \int_{\mathscr{S}} \phi'_\alpha \mathbf{n} \cdot \boldsymbol{\nabla}\lambda \, \mathrm{d}\mathbf{x} + \int_{\mathscr{S}} \alpha \left(\psi \, \mathbf{nn} : \boldsymbol{\nabla}\boldsymbol{\nabla}\phi + \sum_{j=1}^{d-1} \mathbf{t}_j \cdot \boldsymbol{\nabla}(\psi \, \mathbf{t}_j \cdot \boldsymbol{\nabla}\phi) \right) \mathrm{d}\mathbf{x}$$
$$+ \int_{\mathscr{S}} (\lambda + \psi) \, \mathbf{n} \cdot \boldsymbol{\nabla}\phi'_\alpha \, \mathrm{d}\mathbf{x} + \int_{\partial\mathscr{V}\setminus\mathscr{S}} (b\,\psi - \mathbf{n} \cdot \boldsymbol{\nabla}\lambda) \, \phi'_\alpha + (a\,\psi + \lambda) \, \mathbf{n} \cdot \boldsymbol{\nabla}\phi'_\alpha \, \mathrm{d}\mathbf{x} = 0 \tag{22}$$

Hence, if ψ in (22) is set to

$$\psi(\mathbf{x}) = \begin{cases} -\lambda(\mathbf{x}), & \mathbf{x} \in \mathscr{S} \\ -\lambda(\mathbf{x})/a(\mathbf{x}), & \mathbf{x} \in \partial\mathscr{V}\setminus\mathscr{S}, \ a(\mathbf{x}) \neq 0 \\ \mathbf{n} \cdot \boldsymbol{\nabla}\lambda(\mathbf{x})/b(\mathbf{x}), & \mathbf{x} \in \partial\mathscr{V}\setminus\mathscr{S}, \ \text{otherwise} \end{cases}$$

and if λ satisfies the dual problem

$$\Delta\lambda = 0, \quad \mathbf{x} \in \mathscr{V} \tag{23a}$$

$$\mathbf{n} \cdot \boldsymbol{\nabla}\lambda = \sum_{j=1}^{d-1} \mathbf{t}_j \cdot \boldsymbol{\nabla}(p \, \mathbf{t}_j \cdot \boldsymbol{\nabla}\phi), \quad \mathbf{x} \in \mathscr{S} \tag{23b}$$

$$a \, \mathbf{n} \cdot \boldsymbol{\nabla}\lambda + b\lambda = 0, \quad \mathbf{x} \in \partial\mathscr{V}\setminus\mathscr{S} \tag{23c}$$

then

$$I'_\alpha(\mathscr{S}) = -\int_{\mathscr{S}} \alpha \left(\lambda \, \mathbf{nn} : \boldsymbol{\nabla}\boldsymbol{\nabla}\phi + \sum_{j=1}^{d-1} \mathbf{t}_j \cdot \boldsymbol{\nabla}(\lambda \, \mathbf{t}_j \cdot \boldsymbol{\nabla}\phi) \right) \mathrm{d}\mathbf{x} \tag{24}$$

One may note that (24) expresses the induced change in the functional independent of the induced disturbance in the solution.

3.3. *Optimization method*

Due to the absence of the induced disturbance in (24), a descent direction for α can be determined from (13b) and (24) in a straightforward manner. For this purpose, we define the gradient of E with respect to $\mathscr{S}$ by the function $\operatorname{grad} E(\mathscr{S}) : \mathscr{S} \mapsto \mathbb{R}$ with the property:

$$\int_{\mathscr{S}} \alpha(\mathbf{x}) \operatorname{grad} E(\mathscr{S})(\mathbf{x}) \, \mathrm{d}\mathbf{x} = \lim_{\varepsilon \to 0} \frac{1}{\varepsilon} \left[E(\mathscr{S}_{\varepsilon\alpha}) - E(\mathscr{S}) \right] \tag{25}$$

for all suitable α. By (12), (13) and (24), the gradient is readily identified as

$$\operatorname{grad} E(\mathscr{S}) = -\lambda \, \mathbf{nn} : \boldsymbol{\nabla}\boldsymbol{\nabla}\phi - \sum_{j=1}^{d-1} \mathbf{t}_j \cdot \boldsymbol{\nabla}(\lambda \, \mathbf{t}_j \cdot \boldsymbol{\nabla}\phi) - \frac{p^2}{2R} - p \, \mathrm{Fr}^{-2} \mathbf{n} \cdot \mathbf{e}_d \tag{26}$$

From (25) it follows that if $\alpha = -\operatorname{grad} E(\mathscr{S})$ and γ is set to a small positive number, then

$$E(\mathscr{S}_{\gamma\alpha}) - E(\mathscr{S}) = -\gamma \int_{\mathscr{S}} (\operatorname{grad} E(\mathscr{S}))^2 \, \mathrm{d}\mathbf{x} + O(\gamma^2) \leqslant 0 + O(\gamma^2) \tag{27}$$

Therefore, $\alpha = -\operatorname{grad} E(\mathscr{S})$ is a descent direction and $\mathscr{S}_{\gamma\alpha}$ improves on $\mathscr{S}$. The free-surface flow problem can thus be solved by repeating the following operations:

(A1) For given $\mathscr{S}$, solve the primal problem (6) for ϕ.
(A2) Solve the dual problem (23) for λ.
(A3) Determine $\alpha = -\operatorname{grad} E(\mathscr{S})$ from (26).
(A4) Choose the step size $\gamma > 0$ and adjust $\mathscr{S}$ to $\mathscr{S}_{\gamma\alpha}$.

The iterative process (A1)–(A4) is called the adjoint optimization method. The actual free boundary $\mathcal{S}^*$ is obtained if $\operatorname{grad} E(\mathcal{S}^*) = 0$.

The condition $\operatorname{grad} E(\mathcal{S}^*) = 0$ only ensures that a *local* minimum is attained. If the cost functional is non-convex, then multiple local minima can occur. The actual solution to the steady free-surface flow problem is then determined by the *global* minimum. The dynamic condition (3b) implies that the cost functional vanishes for the actual solution. Hence, the correct minimum is identifiable. If the cost functional is indeed non-convex, then it is important that the adjoint optimization method is provided with an initial approximation that is sufficiently close to the actual solution. A prolongated coarse-grid approximation to the solution can serve for this purpose.

4. FOURIER ANALYSIS OF THE OPTIMIZATION PROBLEM

The behaviour of the cost functional in the neighbourhood of a minimum is characterized by the Hessian, i.e. the second derivative of the cost functional with respect to the free boundary. As a result, the properties of the optimization problem and the convergence behaviour of the adjoint optimization method depend on the characteristics of the Hessian. In this section we use Fourier techniques to examine the properties of the Hessian and we consider the implications for the solution behaviour and the posedness of the optimal shape design problem and the convergence behaviour of the adjoint method.

4.1. Hessian of the functional

The behaviour of the cost functional in the neighbourhood of a minimum is characterized by its *Hessian*, which is defined by the function $\operatorname{grad}^2 E(\mathscr{S}) : \mathscr{S} \times \mathscr{S} \mapsto \mathbb{R}$ with the property:

$$\int_{\mathscr{S}} \alpha(\mathbf{y}) \operatorname{grad} E(\mathscr{S})(\mathbf{x}, \mathbf{y}) \, \mathrm{d}\mathbf{y} = \lim_{\varepsilon \to 0} \frac{1}{\varepsilon} [\operatorname{grad} E(\mathscr{S}_{\varepsilon\alpha})(\mathbf{x}) - \operatorname{grad} E(\mathscr{S})(\mathbf{x})] \tag{28}$$

for all suitable α. To show that the properties of the optimization problem are essentially contained in the Hessian, we consider the following expansion of the cost

functional:

$$E(\mathscr{S}_{\varepsilon\alpha}) = E(\mathscr{S}) + \varepsilon \int_{\mathscr{S}} \alpha(\mathbf{x}) \operatorname{grad} E(\mathscr{S})(\mathbf{x})\, \mathrm{d}\mathbf{x} + \frac{\varepsilon^2}{2} \int_{\mathscr{S}} \int_{\mathscr{S}} \alpha(\mathbf{x})\alpha(\mathbf{y}) \operatorname{grad}^2 E(\mathscr{S})(\mathbf{x},\mathbf{y})\, \mathrm{d}\mathbf{y}\, \mathrm{d}\mathbf{x} + O(\varepsilon^3), \quad \text{as } \varepsilon \to 0 \tag{29}$$

Clearly, in order to have a minimum, the gradient must vanish, so that indeed the Hessian determines the behaviour of the cost functional in the neighbourhood of a minimum.

To demonstrate that the Hessian determines the convergence behaviour of the adjoint optimization method, we consider a perturbation $\mathscr{S}^*_{\varepsilon\alpha}$ of the optimal boundary $\mathscr{S}^*$. Because $\operatorname{grad} E(\mathscr{S}^*) = 0$, it follows from (28) that for sufficiently small ε,

$$\operatorname{grad} E(\mathscr{S}^*_{\varepsilon\alpha})(\mathbf{x}) = \varepsilon \int_{\mathscr{S}} \alpha(\mathbf{y}) \operatorname{grad}^2 E(\mathscr{S}^*)(\mathbf{x},\mathbf{y})\, \mathrm{d}\mathbf{y} + O(\varepsilon^2) \tag{30}$$

This implies that in the neighbourhood of the optimum, the Hessian relates the gradient to the disturbance in the free-boundary position. Because the adjoint method uses the gradient to adjust the free boundary, the Hessian determines the change in the error in the boundary position. Hence, the Hessian indeed determines the convergence behaviour of the adjoint optimization method.

4.2. Fourier analysis of the Hessian

The properties of the Hessian can be conveniently examined by means of the Fourier analysis for optimization problems presented in Reference [16]. We perform the analysis for the specific case of a domain $\mathscr{V}^* = \{\mathbf{x} \in \mathbb{R}^d\colon\ -1 < x_d < 0\}$ with free boundary $\mathscr{S}^* = \{\mathbf{x} \in \mathbb{R}^d\colon\ x_d = 0\}$ and fixed boundary $\partial\mathscr{V}^* \backslash \mathscr{S}^* = \{\mathbf{x} \in \mathbb{R}^d : x_d = -1\}$. Recall that x_d is the vertical co-ordinate. Assuming that the fixed boundary is impermeable, a in (6) is set to 1 and b and c are set to 0. The uniform horizontal flow potential $\phi^* = \mathbf{U} \cdot \mathbf{x}$, with $\mathbf{U}$ a constant vector in $\{\mathbf{U} \in \mathbb{R}^d : \|\mathbf{U}\| = 1, U_d = 0\}$, then satisfies the boundary value problem (6). The corresponding solution of the dual problem (23) is $\lambda^* = 0$ and the gradient (26) vanishes, so that $\mathscr{S}^*$ is the optimal boundary. Indeed, the uniform horizontal flow is a solution of the steady free-surface flow problem.

Next, consider the perturbed boundary $\mathscr{S}^*_{\varepsilon\alpha}$. The solutions of the perturbed primal and dual problem are expanded as

$$\phi^*_{\varepsilon\alpha} = \mathbf{U} \cdot \mathbf{x} + \varepsilon \phi'_\alpha(\mathbf{x}) + O(\varepsilon^2) \tag{31a}$$

$$\lambda^*_{\varepsilon\alpha} = 0 + \varepsilon \lambda'_\alpha(\mathbf{x}) + O(\varepsilon^2) \tag{31b}$$

If (31a) and (31b) are inserted in (6) and (23), respectively, and the normal vector to $\mathscr{S}^*_{\varepsilon\alpha}$ is expanded in the same manner as in (10), then collection of terms of $O(\varepsilon)$ reveals that the induced disturbances are governed by:

$$\Delta \phi'_\alpha = 0, \quad \mathbf{x} \in \mathscr{V}^* \tag{32a}$$

$$\mathbf{e}_d \cdot \nabla \phi'_\alpha = 0, \quad \mathbf{x} \in \partial \mathscr{V}^* \backslash \mathscr{S}^* \tag{32b}$$

$$\mathbf{e}_d \cdot \nabla \phi'_\alpha = \mathbf{U} \cdot \nabla \alpha, \quad \mathbf{x} \in \mathscr{S}^* \tag{32c}$$

and

$$\Delta \lambda'_\alpha = 0, \quad \mathbf{x} \in \mathscr{V}^* \tag{33a}$$

$$\mathbf{e}_d \cdot \nabla \lambda'_\alpha = 0, \quad \mathbf{x} \in \partial \mathscr{V}^* \backslash \mathscr{S}^* \tag{33b}$$

$$\mathbf{e}_d \cdot \nabla \lambda'_\alpha = -\mathbf{U} \cdot \nabla (\mathbf{U} \cdot \nabla \phi'_\alpha + \mathrm{Fr}^{-2} \alpha), \quad \mathbf{x} \in \mathscr{S}^* \tag{33c}$$

Moreover, upon inserting (31) in (26), one obtains that the gradient corresponding to the perturbed boundary $\mathscr{S}^*_{\varepsilon\alpha}$ reads

$$\operatorname{grad} E(\mathscr{S}^*_{\varepsilon\alpha}) = \varepsilon (\mathrm{Fr}^{-2} (\mathbf{U} \cdot \nabla \phi'_\alpha + \mathrm{Fr}^{-2} \alpha) - \mathbf{U} \cdot \nabla \lambda'_\alpha) + O(\varepsilon^2) \tag{34}$$

Note that for any perturbation α, the induced disturbances follow from (32) and (33). The gradient corresponding to the perturbed boundary can then be obtained from (34). Because $\operatorname{grad} E(\mathscr{S}^*) = 0$, important information about the Hessian can subsequently be extracted from (28).

The analysis proceeds by assuming α, ϕ'_α and λ'_α to be a linear combination of horizontal Fourier modes. Because (32) through (34) are linear in α, ϕ'_α and λ'_α, it suffices to consider a single mode. Denoting by $\mathbf{k} = k_1 \mathbf{e}_1 + \cdots + k_{d-1} \mathbf{e}_{d-1}$ the horizontal wave-number, α is set to

$$\alpha(\mathbf{x}) = \hat{\alpha}(\mathbf{k}) \exp(\mathrm{i}\mathbf{k} \cdot \mathbf{x}) \tag{35}$$

with $\mathrm{i} = \sqrt{-1}$. The induced disturbances ϕ'_α and λ'_α comply with (32) and (33), respectively, if

$$\phi'_\alpha = \hat{\phi}(\mathbf{k}) \exp(\mathrm{i}\mathbf{k} \cdot \mathbf{x}) \cosh(|\mathbf{k}| (x_d + 1)) \tag{36a}$$

$$\lambda'_\alpha = \hat{\lambda}(\mathbf{k}) \exp(\mathrm{i}\mathbf{k} \cdot \mathbf{x}) \cosh(|\mathbf{k}| (x_d + 1)) \tag{36b}$$

and

$$|\mathbf{k}| \sinh |\mathbf{k}| \, \hat{\phi}(\mathbf{k}) = \mathrm{i}\mathbf{k} \cdot \mathbf{U} \, \hat{\alpha}(\mathbf{k}) \tag{37a}$$

$$|\mathbf{k}| \sinh |\mathbf{k}| \, \hat{\lambda}(\mathbf{k}) = -\mathrm{i}\mathbf{k} \cdot \mathbf{U} (\mathrm{i}\mathbf{k} \cdot \mathbf{U} \cosh |\mathbf{k}| \, \hat{\phi}(\mathbf{k}) + \mathrm{Fr}^{-2} \, \hat{\alpha}(\mathbf{k})) \tag{37b}$$

Recalling that $\operatorname{grad} E(\mathscr{S}^*) = 0$, by (34) through (37), the change in the gradient satisfies

$$\lim_{\varepsilon \to 0} \frac{1}{\varepsilon} [\operatorname{grad} E(\mathscr{S}^*_{\varepsilon\alpha}) - \operatorname{grad} E(\mathscr{S}^*)] = \hat{H}(\mathbf{k}) \, \hat{\alpha}(\mathbf{k}) \exp(\mathrm{i}\mathbf{k} \cdot \mathbf{x}) \tag{38}$$

with

$$\hat{H}(\mathbf{k}) = \left(\mathrm{Fr}^{-2} - \frac{(\mathbf{k} \cdot \mathbf{U})^2}{|\mathbf{k}| \tanh |\mathbf{k}|} \right)^2 \tag{39}$$

The object $\hat{H}(\mathbf{k})$ is referred to as the Fourier symbol of the Hessian.

4.3. Properties of the optimization problem

The Fourier symbol of the Hessian contains important information about the posedness and the solution behaviour of the optimization problem. To illustrate this, we consider the Fourier transform of the perturbation $\alpha(\mathbf{x})$ and its inverse

$$\hat{\alpha}(\mathbf{k}) = (2\pi)^{1-d} \int_{\mathscr{S}^*} \alpha(\mathbf{x}) \exp(-\mathrm{i}\mathbf{k}\cdot\mathbf{x})\,\mathrm{d}\mathbf{x}, \quad \alpha(\mathbf{x}) = \int_{-\infty}^{\infty} \hat{\alpha}(\mathbf{k})\, \exp(\mathrm{i}\mathbf{k}\cdot\mathbf{x})\,\mathrm{d}\mathbf{k} \tag{40}$$

From (28) and (38) it then follows that

$$\int_{\mathscr{S}^*} \alpha(\mathbf{y}) \operatorname{grad}^2 E(\mathscr{S}^*)(\mathbf{x},\mathbf{y})\,\mathrm{d}\mathbf{y} = \int_{-\infty}^{\infty} \hat{H}(\mathbf{k})\,\hat{\alpha}(\mathbf{k}) \exp(\mathrm{i}\mathbf{k}\cdot\mathbf{x})\,\mathrm{d}\mathbf{k} \tag{41}$$

Hence, by (29), if terms of $O(\varepsilon^3)$ are ignored, the change in the cost functional due to the perturbation of the free boundary reads:

$$\begin{aligned}
E(\mathscr{S}^*_{\varepsilon\alpha}) - E(\mathscr{S}^*) &= \frac{\varepsilon^2}{2} \int_{\mathscr{S}} \alpha(\mathbf{x}) \int_{\mathscr{S}} \alpha(\mathbf{y}) \operatorname{grad}^2 E(\mathscr{S}^*)(\mathbf{x},\mathbf{y})\,\mathrm{d}\mathbf{y}\,\mathrm{d}\mathbf{x} \\
&= \frac{\varepsilon^2}{2} \int_{\mathscr{S}} \alpha(\mathbf{x}) \int_{-\infty}^{\infty} \hat{H}(\mathbf{k})\,\hat{\alpha}(\mathbf{k})\, \exp(\mathrm{i}\mathbf{k}\cdot\mathbf{x})\,\mathrm{d}\mathbf{k}\,\mathrm{d}\mathbf{x} \\
&= \frac{\varepsilon^2}{2} \int_{-\infty}^{\infty} \hat{H}(\mathbf{k})\,\hat{\alpha}(\mathbf{k}) \int_{\mathscr{S}} \alpha(\mathbf{x}) \exp(\mathrm{i}\mathbf{k}\cdot\mathbf{x})\,\mathrm{d}\mathbf{x}\,\mathrm{d}\mathbf{k} \\
&= \frac{\varepsilon^2}{2} (2\pi)^{d-1} \int_{-\infty}^{\infty} \hat{H}(\mathbf{k})\,\hat{\alpha}(\mathbf{k})\,\overline{\hat{\alpha}(\mathbf{k})}\,\mathrm{d}\mathbf{k} \\
&= \frac{\varepsilon^2}{2} (2\pi)^{d-1} \int_{-\infty}^{\infty} \hat{H}(\mathbf{k})\,|\hat{\alpha}(\mathbf{k})|^2\,\mathrm{d}\mathbf{k}
\end{aligned} \tag{42}$$

with $\overline{\hat{\alpha}(\mathbf{k})}$ the complex conjugate of $\hat{\alpha}(\mathbf{k})$. Equation (42) implies that $\hat{H}(\mathbf{k})$ expresses the ability of the optimization problem to distinguish between a boundary $\mathscr{S}^*$ and a perturbed boundary $\mathscr{S}^*_{\varepsilon\alpha}$, with $\alpha(\mathbf{x})$ a Fourier component with wave number $\mathbf{k}$.

To illustrate the behaviour of the Fourier symbol $\hat{H}(\mathbf{k})$, we consider (39) for $\mathbf{k}\in\mathbb{R}^2$ (i.e. $d=3$). Without loss of generality, we assume that $\mathbf{U}=\mathbf{e}_1$, so that $\mathbf{k}\cdot\mathbf{U}=k_1$. Figure 1 then displays contours of $\mathrm{Fr}^{-2}\pm\sqrt{\hat{H}(\mathbf{k})}$, e.g. if $\mathrm{Fr}=\frac{1}{2}$, then $\mathrm{Fr}^{-2}\pm\sqrt{\hat{H}(\mathbf{k})}=4$ is the contour for which $\hat{H}(\mathbf{k})=0$ and $\mathrm{Fr}^{-2}\pm\sqrt{\hat{H}(\mathbf{k})}\in\{0,8\}$ are the contours for which $\hat{H}(\mathbf{k})=16$.

The solution behaviour of the shape optimization problem is determined by the *critical modes*, i.e. the wave numbers for which $\hat{H}(\mathbf{k})$ vanishes. These critical modes yield a change in the cost functional of just $O(\varepsilon^3)$, instead of $O(\varepsilon^2)$. Hence, a small perturbation of the uniform free-surface flow is composed of a linear combination of the critical modes. It is important to observe that to each Froude number corresponds a curve of critical wave numbers. The critical modes are associated with steady surface gravity waves; see, e.g. References [17, 19]. Note that for $d=2$ ($k_2=0$) and $\mathrm{Fr}<1$, the condition $\hat{H}(k_c)=0$ yields a unique relation between

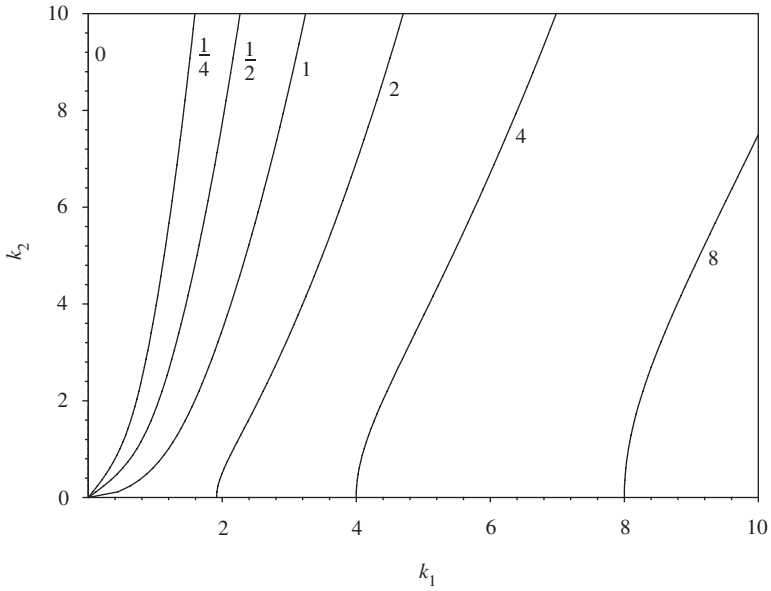

Figure 1. Contours of $\mathrm{Fr}^{-2} \pm \sqrt{\hat{H}(\mathbf{k})}$.

the wave number of the surface gravity wave and the Froude number. For $d = 2$ and $\mathrm{Fr} \geqslant 1$, critical modes are absent and steady surface gravity waves do not occur.

The Fourier symbol of the Hessian also gives information about the posedness of the optimization problem. The optimization problem is said to be well posed if it has a unique solution that is stable to perturbations in the auxiliary data. Uniqueness is ensured if $\hat{H}(\mathbf{k}) > 0$ for all $\mathbf{k}$. From the above considerations, it is clear that uniqueness cannot be ensured. However, this does not necessarily imply that the optimization problem is ill posed. It merely implies that the behaviour of critical modes is not described by the above theory. Linear stability of the optimization problem generally demands that

$$\hat{H}(\mathbf{k}) = O(|\mathbf{k}|^{\theta}), \quad \text{as } |\mathbf{k}| \to \infty \tag{43}$$

for some $\theta \geqslant 0$; see Reference [16]. This requirement expresses that the optimization problem clearly notices high wave-number perturbations of the free boundary. Unfortunately, if $\mathbf{k} \in \mathbb{R}^2$, the contours on which $\hat{H}(\mathbf{k}) = 0$ contain waves with $|\mathbf{k}| \to \infty$. Hence, the linear theory is insufficient to establish the stability of the three dimensional free-surface flow problem. However, such waves do not occur for $d = 2$ and, therefore, linear stability of the two dimensional optimization problem is ensured.

4.4. Stability of the adjoint method

To examine the stability of the adjoint method, we consider a perturbation $\mathscr{S}^*_{\varepsilon\alpha}$ of the optimal free boundary $\mathscr{S}^*$. One iteration of the adjoint optimization method yields a new

approximation $\mathscr{S}^*_{\varepsilon\underline{\alpha}}$, with

$$\varepsilon\underline{\alpha}(\mathbf{x}) = \varepsilon\alpha(\mathbf{x}) - \gamma \operatorname{grad} E(\mathscr{S}^*_{\varepsilon\alpha})(\mathbf{x}) \tag{44}$$

for some step-size $\gamma > 0$. Hence, by (30), $\underline{\alpha}$ and α are related in the following manner:

$$\underline{\alpha}(\mathbf{x}) = \alpha(\mathbf{x}) - \gamma \int_{\mathscr{S}} \alpha(\mathbf{y}) \operatorname{grad}^2 E(\mathscr{S}^*)(\mathbf{x},\mathbf{y})\, \mathrm{d}\mathbf{y} \tag{45}$$

The *contraction number* ζ of the adjoint method is defined by the reduction of the error in the free-boundary position between successive iterations, i.e.

$$\zeta = \sup_{\alpha} \frac{\|\alpha(\mathbf{x}) - \gamma \int_{\mathscr{S}^*} \alpha(\mathbf{y}) \operatorname{grad}^2 E(\mathscr{S}^*)(\mathbf{x},\mathbf{y})\, \mathrm{d}\mathbf{y}\|}{\|\alpha(\mathbf{x})\|} \tag{46}$$

where the supremum is taken over all admissible functions $\alpha(\mathbf{x})$. Because $\|\underline{\alpha}\| \leqslant \zeta\|\alpha\|$, stability of the adjoint method is ensured if $\zeta \leqslant 1$.

If the L_2 norm is implied in (46), we can use (41) and Parseval's identity to recast (46) into:

$$\zeta = \sup_{\hat{\alpha}} \left(\frac{\int_{-\infty}^{\infty} (1 - \gamma \hat{H}(\mathbf{k}))^2 \, |\hat{\alpha}(\mathbf{k})|^2 \, \mathrm{d}\mathbf{k}}{\int_{-\infty}^{\infty} |\hat{\alpha}(\mathbf{k})|^2 \, \mathrm{d}\mathbf{k}} \right)^{1/2} \tag{47}$$

If problem (7) is solved numerically, then the infinite domain is usually truncated and $\alpha(\mathbf{x})$ is represented on a grid. In that case, if $\boldsymbol{\ell} = (\ell_1, \ldots, \ell_{d-1})$ is the horizontal length of the truncated domain and $\mathbf{h} = (h_1, \ldots, h_{d-1})$ is the horizontal mesh width of the grid, then we only have to consider isolated wave numbers in the set

$$\mathscr{W}_{\mathbf{h}} = \{\mathbf{k} : k_j = n\pi/\ell_j, n = \pm 1, \pm 2, \ldots, |k_j| \leqslant \pi/h_j\} \tag{48}$$

see Figure 2 for an illustration. It follows from (47) that ζ is then given by

$$\zeta = \sup_{\mathbf{k} \in \mathscr{W}_{\mathbf{h}}} |1 - \gamma \hat{H}(\mathbf{k})| \tag{49}$$

Stability of the adjoint optimization method is ensured if the right hand side of (49) is at most 1. This can be accomplished by choosing the step size γ according to

$$\gamma = c \left(\sup_{\mathbf{k} \in \mathscr{W}_{\mathbf{h}}} \hat{H}(\mathbf{k}) \right)^{-1} \tag{50}$$

for some constant $c \in]0, 2[$.

The supremum of $\hat{H}$ in $\mathscr{W}_{\mathbf{h}}$ is for well posed problems determined by the highest wave-number components in $\mathscr{W}_{\mathbf{h}}$; refer to (43). From (48) it follows that the highest wave number in $\mathscr{W}_{\mathbf{h}}$ is $O(1/|\mathbf{h}|)$. Hence, in general, the step size diminishes as $\gamma = O(|\mathbf{h}|^{\theta})$ as $|\mathbf{h}| \to 0$. In particular, for the Fourier symbol (39), if the grid is refined in such a manner that $\mathbf{h} = |\mathbf{h}|\mathbf{c}$ as $|\mathbf{h}| \to 0$, with $\mathbf{c}$ a constant vector, then the supremum of $\hat{H}(\mathbf{k})$ in $\mathscr{W}_{\mathbf{h}}$ is $O(|\mathbf{h}|^{-2})$. The step size must then comply with

$$\gamma = O(|\mathbf{h}|^2) \quad \text{as } |\mathbf{h}| \to 0 \tag{51}$$

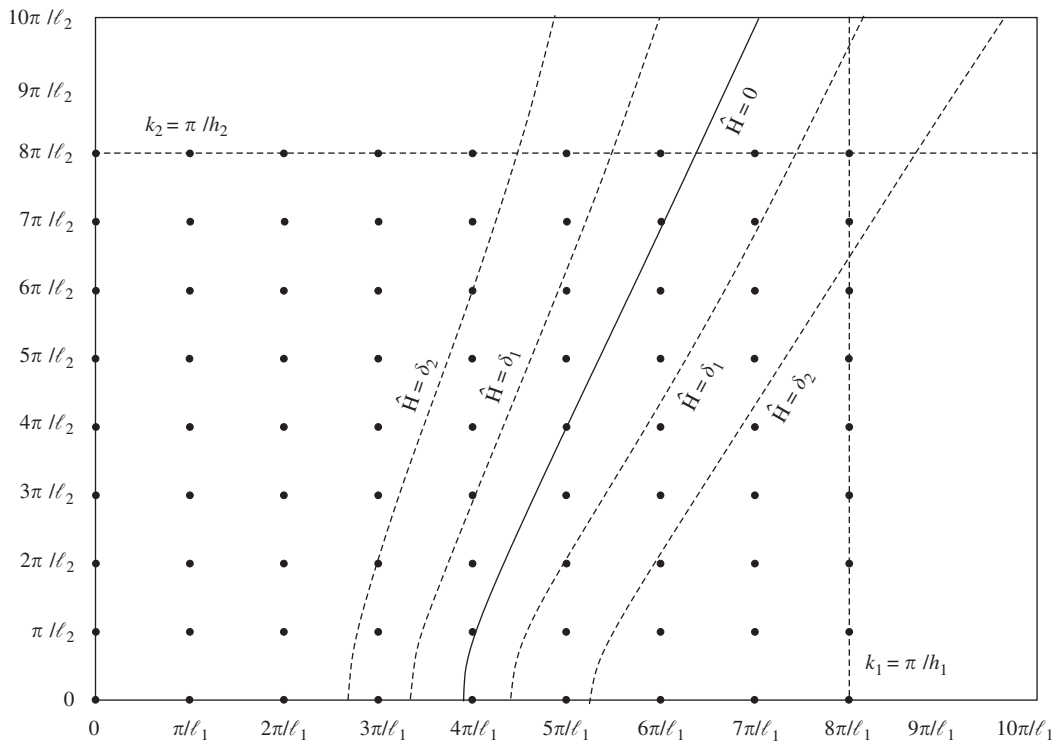

Figure 2. Illustration of the set of wave numbers $\mathscr{W}_{\mathbf{h}}$ (dots) and $\hat{H}(\mathbf{k}) = 0$, $\hat{H}(\mathbf{k}) = \delta_{1,2}$.

to maintain stability of the oscillatory modes, i.e. the modes with large $|\mathbf{k}|$. This implies that the step size in the adjoint optimization method must be reduced as the spatial grid is refined to maintain stability of the high wave-number components.

4.5. *Convergence of the adjoint method*

The convergence behaviour of an iterative method is usually characterized by its contraction number. However, this characterization is inappropriate for problems with critical modes ($\hat{H}(\mathbf{k}) = 0$) and dispersive behaviour, such as the considered free-surface flow problem. The contraction number is based on the behaviour of isolated waves, whereas for dispersive problems the behaviour of *wave groups* is relevant; see, e.g. References [17, 21]. This distinction is essential if critical modes occur. As a result of the critical modes, the contraction number indicates that convergence lacks. However, due to the dispersive properties of the problem, this indication is too pessimistic.

To determine the convergence behaviour of the adjoint optimization method (A1)–(A4), we reconsider the perturbation $\mathscr{S}^*_{\varepsilon\alpha}$ of the optimal free boundary $\mathscr{S}^*$. The Fourier components of the perturbation can be separated into a contribution $\hat{\rho}(\mathbf{k})$ of the modes in the neighbourhood

of the critical modes and a remainder:

$$\hat{\alpha}(\mathbf{k}) = \hat{\rho}(\mathbf{k}) + (\hat{\alpha}(\mathbf{k}) - \hat{\rho}(\mathbf{k})) \tag{52a}$$

where $\hat{\rho}(\mathbf{k}) = \hat{w}(\mathbf{k})\,\hat{\alpha}(\mathbf{k})$,

$$\hat{w}(\mathbf{k}) = \begin{cases} 1 & \text{if } \hat{H}(\mathbf{k}) \leqslant \delta_1 \\ 0 & \text{if } \hat{H}(\mathbf{k}) \geqslant \delta_2 \end{cases} \tag{52b}$$

and $\delta_{1,2}$ are constants such that $\delta_2 > \delta_1 > 0$; see the illustration in Figure 2. The transition of $\hat{w}(\mathbf{k})$ from 1 to 0 can be constructed in any suitable manner and is largely arbitrary. However, below $\hat{\rho}(\mathbf{k})$ is required to be an analytic function.

Denoting by $\varepsilon\alpha_n(\mathbf{x})$ the disturbance in the free-boundary position after n iterations of the adjoint method, we obtain from (41) and (45):

$$\hat{\alpha}_n(\mathbf{k}) = (1 - \gamma\hat{H}(\mathbf{k}))^n \hat{\alpha}(\mathbf{k}) \tag{53}$$

Hence, it follows from (52) that

$$\alpha_n(\mathbf{x}) = \int_{-\infty}^{\infty} (1 - \gamma\hat{H}(\mathbf{k}))^n \hat{\rho}(\mathbf{k}) \exp(\mathrm{i}\mathbf{k}\cdot\mathbf{x})\,\mathrm{d}\mathbf{k} + O(|1 - \gamma\delta_1|^n) \tag{54}$$

Because $|1 - \gamma\delta_1| < 1$, the remainder vanishes exponentially as $n \to \infty$. This implies that the asymptotic behaviour of $\alpha_n(\mathbf{x})$ for large n is determined by the Fourier components in the neighbourhood of the critical modes.

From (54) it follows that if $\hat{\rho}_n(\mathbf{k})$ is defined recursively by

$$\hat{\rho}_0(\mathbf{k}) = \hat{\rho}(\mathbf{k}) \tag{55a}$$

$$\hat{\rho}_n(\mathbf{k}) = (1 - \gamma\hat{H}(\mathbf{k}))\hat{\rho}_{n-1}(\mathbf{k}), \quad n = 1, 2, \ldots \tag{55b}$$

then $\alpha_n(\mathbf{x}) \sim \rho_n(\mathbf{x})$ as $n \to \infty$. Equation (55b) can be recast into:

$$\frac{\hat{\rho}_{n+1}(\mathbf{k}) - \hat{\rho}_n(\mathbf{k})}{\gamma} + \hat{H}(\mathbf{k})\,\hat{\rho}_n(\mathbf{k}) = 0 \tag{56}$$

Note that for sufficiently small γ, the first term can be conceived as a difference approximation to the derivative of $\hat{\rho}_n(\mathbf{k})$ with respect to *pseudo time* $n\gamma$. We assume that $\hat{\rho}_n(\mathbf{k}) \sim \exp(\tau n\gamma)\hat{\rho}_0(\mathbf{k})$ as $n \to \infty$. Equation (56) then implies

$$(\exp(\tau\gamma) - 1)/\gamma + \hat{H}(\mathbf{k}) = 0 \tag{57}$$

Taylor expansion of $\exp(\tau\gamma)$ yields

$$\tau = -\hat{H}(\mathbf{k}) \tag{58}$$

provided that $O(\tau^2)$ terms are negligible. By (52b), $\hat{H}(\mathbf{k}) \leqslant \delta_2$. Hence, if δ_2 is chosen sufficiently small, the $O(\tau^2)$ terms in the Taylor expansion can indeed be ignored. Equation (58) relates the pseudo time behaviour of a disturbance in the free-boundary position to its spatial

behaviour. Therefore, it appears appropriate to refer to (58) as the *dispersion relation* of the adjoint method.

From (54) to (58) it follows that as $n\gamma \to \infty$,

$$\alpha_n(\mathbf{x}) \sim \int_{-\infty}^{\infty} \hat{\rho}(\mathbf{k})\, \exp(\mathrm{i}\Omega(\mathbf{k})\, n\gamma)\, \mathrm{d}\mathbf{k} \tag{59}$$

with

$$\Omega(\mathbf{k}) = \mathrm{i}\hat{H}(\mathbf{k}) + \frac{\mathbf{k}\cdot\mathbf{x}}{n\gamma} \tag{60}$$

The integral in (59) vanishes exponentially as $n\gamma \to \infty$, except near stationary critical points of $\hat{H}(\mathbf{k})$, i.e. the wave numbers $\mathbf{k}_0$ such that

$$\hat{H}(\mathbf{k}_0) = 0, \quad \frac{\partial \hat{H}}{\partial k_j}(\mathbf{k}_0) = 0 \tag{61}$$

Each stationary critical point yields a contribution

$$\hat{\rho}(\mathbf{k}_0)\left(\frac{2\pi}{n\gamma}\right)^{(d-1)/2}\left(\det\left|\frac{\partial^2 \hat{H}}{\partial k_i \partial k_j}(\mathbf{k}_0)\right|\right)^{-1/2} \exp(\mathrm{i}\mathbf{k}_0\cdot\mathbf{x} + \mathrm{i}\xi) \tag{62}$$

with ξ a multiple of $\pi/4$, depending on the properties of $\partial^2\hat{H}/\partial k_i \partial k_j$. The above can be proved by the method of stationary phase; see, e.g. References [21, 22].

Due to the quadratic form of (39), any critical point is a stationary point as well. Hence, if we define the *evaluation error* e_n by the L_2 norm of the error in the boundary position, i.e. $\mathsf{e}_n \equiv \|\varepsilon\alpha_n\|$, then we anticipate that the adjoint method yields the following asymptotic convergence behaviour:

$$\mathsf{e}_n = O(\zeta^{n\gamma}) \quad \text{if } \forall \mathbf{k} : \hat{H}(\mathbf{k}) > 0 \tag{63a}$$

$$\mathsf{e}_n = O((n\gamma)^{(1-d)/2}) \quad \text{if } \exists \mathbf{k} : \hat{H}(\mathbf{k}) = 0 \tag{63b}$$

as $n \to \infty$, for some constant ζ in $]0, 1[$. The implications of (63) for the convergence behaviour of the adjoint method are summarized in Table I.

Table I. Convergence behaviour of the adjoint method: asymptotic behaviour of the evaluation error e_n for sub- and supercritical flow in 2D and 3D, with n the iteration counter, γ the step size and ζ a constant in $]0, 1[$.

	$d = 2$	$d = 3$
Subcritical	$O(1/\sqrt{n\gamma})$	$O(1/(n\gamma))$
Supercritical	$O(\zeta^{n\gamma})$	$O(1/(n\gamma))$

5. PRECONDITIONING

The asymptotic error behaviour (63) and the stability condition (51) imply that the performance of the adjoint optimization method deteriorates with decreasing mesh width. This deficiency of the method can be repaired by means of preconditioning. This section outlines the preconditioning operation.

5.1. Reconsideration of objectives

To introduce the preconditioning operation, we consider the gradient of the cost functional at a perturbation $\mathscr{S}^*_{\varepsilon\alpha}$ of the optimal boundary $\mathscr{S}^*$. By (38), the Fourier components of the gradient read:

$$\widehat{\operatorname{grad} E(\mathscr{S}^*_{\varepsilon\alpha})}(\mathbf{k}) = \varepsilon \hat{H}(\mathbf{k})\, \hat{\alpha}(\mathbf{k}) \tag{64}$$

Equation (64) implies that for problems that are stable according to (43) with θ strictly positive, the gradient primarily contains highly oscillatory modes (large $|\mathbf{k}|$). Consequently, the adjoint optimization method effectively reduces the cost functional by removing the highly oscillatory disturbances in the boundary position. However, smooth error components are inadequately resolved.

In general, one is interested in obtaining the free-boundary position rather than minimizing the cost functional. If the objective is indeed to obtain the free boundary, then the gradient is unsuitable for adjusting the boundary position.

5.2. General outline

The aim of preconditioning is to restore the relation between the boundary adjustment and the error in the boundary position. An accurate approximation to the error in the free-boundary position can be recovered from the gradient by solving

$$P\beta = \operatorname{grad} E(\mathscr{S}^*_{\varepsilon\alpha}) \tag{65}$$

where P is any convenient operator of which the Fourier symbol satisfies

$$\hat{H}(\mathbf{k}) \leqslant \hat{P}(\mathbf{k}) \quad \text{for all } \mathbf{k} \tag{66a}$$

$$\lim_{|\mathbf{k}| \to \infty} \hat{H}(\mathbf{k})/\hat{P}(\mathbf{k}) = C, \quad \text{for some } C \in]\,0, 1] \tag{66b}$$

The operator P simulates the relation between the gradient and the disturbance in the boundary position. The Fourier components $\hat{\beta}(\mathbf{k})$ are related to the components of the disturbance by

$$\hat{\beta}(\mathbf{k}) = (\hat{H}(\mathbf{k})/\hat{P}(\mathbf{k}))\, \hat{\alpha}(\mathbf{k}) \tag{67}$$

Therefore, $\beta(\mathbf{x})$ is an accurate approximation to $\alpha(\mathbf{x})$ if $\hat{H}(\mathbf{k})/\hat{P}(\mathbf{k}) \approx 1$.

If the adjoint method uses $\beta(\mathbf{x})$ instead of the gradient to displace the free-boundary, then the corresponding stability condition reads:

$$|1 - \gamma \hat{H}(\mathbf{k})/\hat{P}(\mathbf{k})| \leqslant 1 \tag{68}$$

Requirement (66a) ensures that $\hat{H}/\hat{P} \leqslant 1$ for all $\mathbf{k}$, so that the step size γ in the preconditioned method can be set to 1. Consequently, if the problem is solved numerically, the convergence behaviour of the preconditioned method is independent of the mesh width of the applied grid. Condition (66b) makes certain that all Fourier components that are present in the boundary disturbance are also present in the correction, so that the error indeed vanishes as the iteration progresses.

It is important that the numerical methods for solving (65) do not reintroduce the mesh-width dependence. In general, preconditioners P can be constructed for which efficient solution methods, e.g. multigrid methods [23, 24], are available.

5.3. *A preconditioner for 2D free-surface flows*

The construction of the preconditioner from its symbol relies on the theory of pseudo-differential operators; see also Reference [25]. In this section we set up a preconditioner for the 2D steady free-surface flow problem. It is anticipated that a preconditioner for 3D free-surface flows can be constructed similarly.

In two dimensions, the free-boundary is one dimensional and the considered wave number is $k \in \mathbb{R}$. Without loss of generality, we assume that the velocity is scaled such that $U = 1$ in (39). To derive the preconditioner, we first consider the asymptotic behaviour of (39) for large k:

$$\hat{H}(k) \sim k^2, \quad \text{as } k \to \infty \tag{69}$$

The Fourier symbol $-k^2$ corresponds to a Laplace operator. An operator which has the desired behaviour for high wave number components is

$$P_{\mathrm{H}}\,\beta = (\mathrm{Fr}^{-2} - 1)^2 \beta - \frac{\partial^2 \beta}{\partial t^2} \tag{70}$$

where $\partial/\partial t$ denotes the tangential derivative along the free boundary. The Fourier symbol of (70) is

$$\hat{P}_{\mathrm{H}}(k) = (\mathrm{Fr}^{-2} - 1)^2 + k^2 \tag{71}$$

Indeed, $\hat{P}_{\mathrm{H}}(k) \sim k^2$ as $k \to \infty$. Figure 3 compares the Fourier symbols $\hat{P}_{\mathrm{H}}$ and $\hat{H}$. The behaviour of $\hat{P}_{\mathrm{H}}$ closely resembles that of $\hat{H}$ at high wave numbers. Hence, P_{H} accurately recovers highly oscillatory errors in the boundary position. Moreover, P_{H} eliminates the mesh-width dependence of the step size.

The Fourier symbols $\hat{P}_{\mathrm{H}}$ and $\hat{H}$ differ markedly at low wave numbers if $\mathrm{Fr} < 1$. For $\mathrm{Fr} < 1$, the low wave-number behaviour of $\hat{H}$ is accurately approximated by:

$$\hat{P}_{\mathrm{L}}(k) = (1 - (2 - 2\mu)(k/k_0)^2 + (1 - \mu)(k/k_0)^4)(\mathrm{Fr}^{-2} - 1)^2 \tag{72}$$

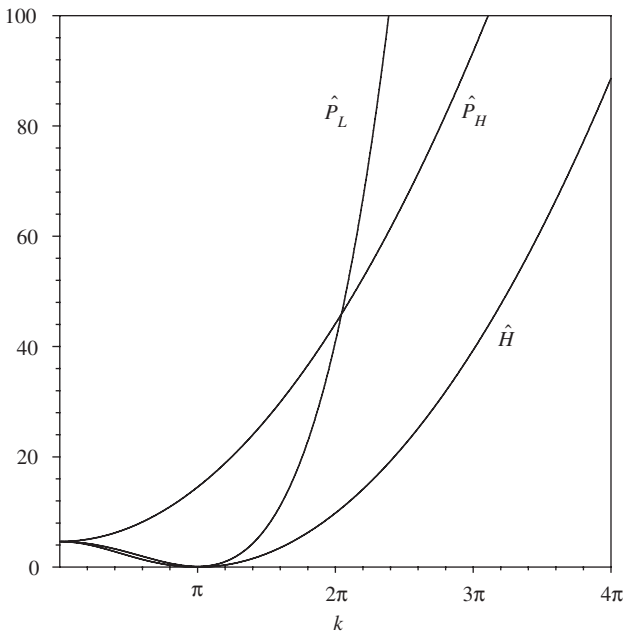

Figure 3. Fourier symbols $\hat{P}_{\mathrm{L}}(k)$, $\hat{P}_{\mathrm{H}}(k)$ and $\hat{H}(k)$ for $\mathrm{Fr} = \sqrt{\tanh(\pi)/\pi}$.

with k_0 the critical wave number of (39) and μ a small positive constant; see Figure 3. The symbol $\hat{P}_{\mathrm{L}}(k)$ corresponds to the differential operator

$$P_{\mathrm{L}}\beta = (\mathrm{Fr}^{-2} - 1)^2 \left(\beta + \frac{2 - 2\mu}{k_0^2} \frac{\partial^2 \beta}{\partial t^2} + \frac{1 - \mu}{k_0^4} \frac{\partial^4 \beta}{\partial t^4} \right) \tag{73}$$

The constant μ ensures that the polynomial $\hat{P}_{\mathrm{L}}(k)$ has no real roots. This is a prerequisite for stability of the preconditioner. Unfortunately, it also implies that the preconditioner leaves the root of $\hat{H}$ undisturbed, i.e. $\hat{H}(k)/\hat{P}_{\mathrm{L}}(k) = 0$ for critical modes. Hence, the asymptotic convergence behaviour (63b) is not essentially improved.

Summarizing, for supercritical flows an effective correction of the free-boundary can be obtained from (65) and (70). The mesh-width dependence of the convergence behaviour is then eliminated. For subcritical flows, the correction is a combination of a high wave-number correction β_{H} from (65), (70) and a low wave-number correction β_{L} from (65), (73), e.g. $(\beta_{\mathrm{L}} + \beta_{\mathrm{H}})/2$. The mesh-width dependence of the convergence behaviour is then removed. However, the asymptotic convergence behaviour is not improved, because the preconditioning does not remove the critical modes.

6. NUMERICAL EXPERIMENTS

The preconditioned adjoint optimization method is tested for two dimensional sub- and supercritical flow over an obstacle in a channel of unit depth at $\mathrm{Fr} = 0.43$ and 2.05. The geometry

of the obstacle is

$$y(x) = -1 + \frac{27}{4}\frac{H}{L^3}x(x-L)^2, \quad 0 \leqslant x \leqslant L \tag{74}$$

with H and L the (non-dimensionalized) height and length of the obstacle, respectively. We choose $H = 0.2$, $L = 2$ for the subcritical test case and $H = 0.44$ and $L = 4.4$ for the supercritical test case, in accordance with the experimental setup from Reference [26]. In addition, we consider the subcritical test case with $H = 0.1$, $L = 2$ and the supercritical test case with $H = 0.22$ and $L = 4.4$.

The boundary value problems (7) and (23) are discretized with bilinear finite elements. The differential operators in the gradient (26) are discretized with central differences. The resulting discrete optimization problem is unstable and displays odd/even oscillations. These are simply removed by smoothing the gradient with the biharmonic operator. For subcritical flows ($\mathrm{Fr} < 1$), a radiation condition must be imposed to avoid non-physical upstream waves; cf. Section 2.1. The upstream waves are eliminated by smoothing the gradient upstream of the obstacle with the Laplace operator, and by applying the low wave number preconditioner P_{L} only downstream.

The numerical experiments are performed on grids with horizontal mesh width $h \in \{L/36, L/72\}$ and vertical mesh width $\frac{1}{24}$. For the supercritical test case, the correction is computed using (65) and (70). For the subcritical test case, the upstream correction is determined in the same manner and the downstream correction is taken as $(\beta_{\mathrm{L}} + \beta_{\mathrm{H}})/2$, with β_{H} from (65), (70) and β_{L} from (65), (73). The constant μ in (73) is set to 0.025. In all cases the step size $\gamma = 1$ is employed.

For the supercritical test case, Figure 4 plots the L_2 norm of the correction after n iterations, $\|\beta_n\|$, versus the iteration counter. The correction behaves as $\|\beta_n\| = O(\zeta^n)$, for some constant $\zeta \in]0, 1[$. The norm of the evaluation error after n iterations can be bounded by

$$\mathsf{e}_n \leqslant \sum_{j=n}^{\infty} \|\beta_j\| \tag{75}$$

It follows from (75) that the evaluation error converges as $O(\zeta^n)$ as well. This is in accordance with the entry in Table I. From Figure 4 we obtain $\zeta \approx 0.35$ for $H = 0.22$ and $\zeta \approx 0.5$ for $H = 0.44$. One may note that the convergence behaviour is indeed independent of the mesh width. Figure 5 compares the computed surface elevation with measurements from Reference [26] for the supercritical test case. The computed result agrees well with the measurements.

For the subcritical test case, $\|\beta_n\|$ is plotted versus n in Figure 6. Note that Figure 6 is a log–log plot. In this case, $\|\beta_n\|$ behaves as $O(n^{-\sigma})$, with $\sigma \approx 1.5$ for $H = 0.1$ and $\sigma \approx 1.2$ for $H = 0.2$. It follows from (75) that the convergence behaviour of the evaluation error is approximately $O(n^{-0.5})$ for $H = 0.1$ and $O(n^{-0.2})$ for $H = 0.2$. Hence, the test case with $H = 0.1$ confirms the entry in Table I. The deteriorated converge behaviour for $H = 0.2$ can be attributed to apparent non-linear behaviour. One may note that the convergence behaviour is virtually independent of the mesh width. Figure 7 compares the computed surface elevation with measurements from Reference [26] for the subcritical test case. The surface elevation displays typical non-linear effects, such as sharp wave crests and wave-length reduction. The amplitude of the computed result is overestimated. However, the overestimation of the

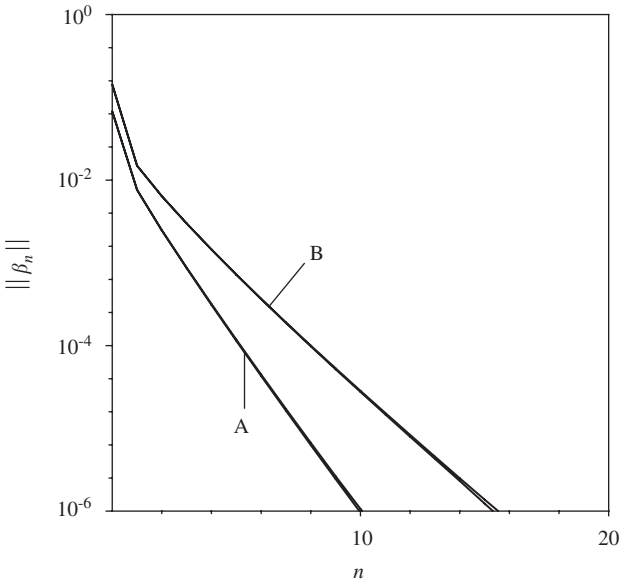

Figure 4. Supercritical test case: norm of the correction versus the iteration counter for $H = 0.22$ (A) and $H = 0.44$ (B) ($h = L/36$ and $h = L/72$ coincide).

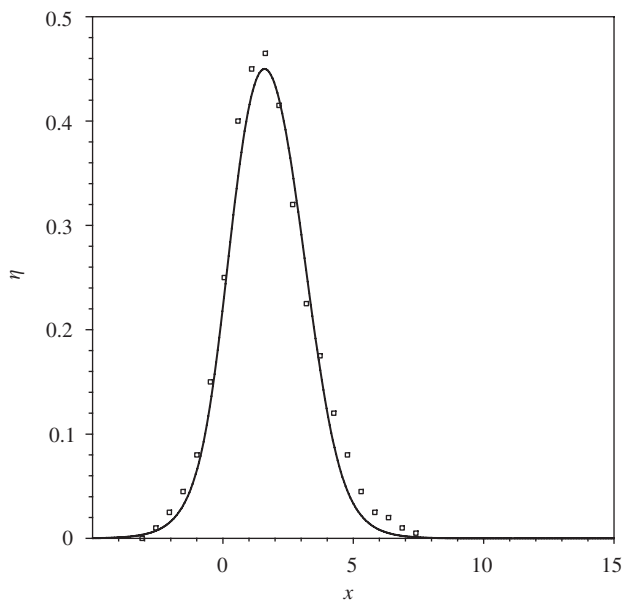

Figure 5. Supercritical test case: computed surface elevation with $H = 0.44$ and $h = L/72$ (*solid line*) and measurements from Reference [26] (*markers only*).

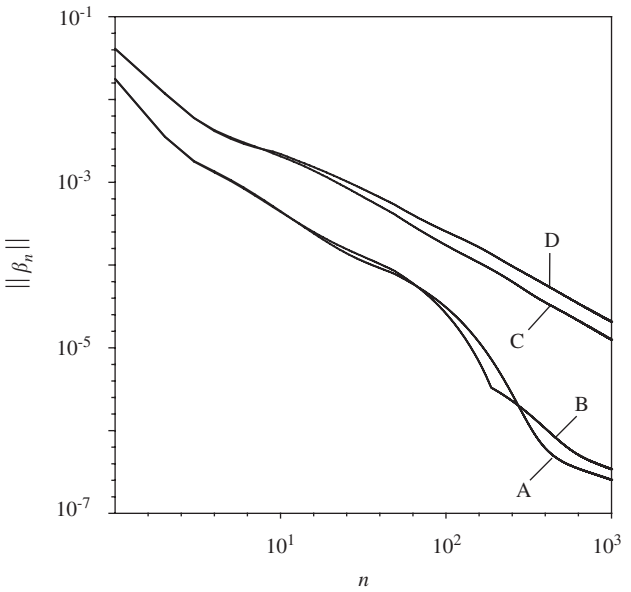

Figure 6. Subcritical test case: norm of the correction versus the iteration counter for $H = 0.1$, $h = L/36$ (A), $h = L/72$ (B) and $H = 0.2$, $h = L/36$ (C), $h = L/72$ (D).

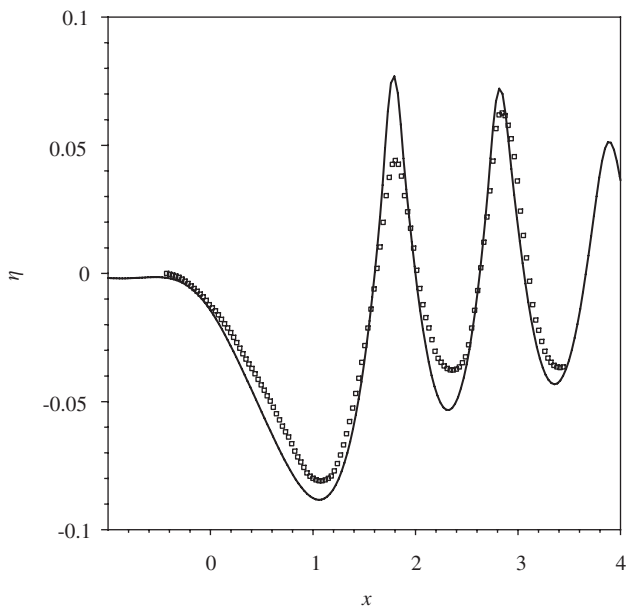

Figure 7. Subcritical test case: computed surface elevation with $H = 0.2$ and $h = L/72$ (*solid line*) and measurements from Reference [26] (*markers only*).

amplitude of the trailing wave is not unusual; see, for instance, References [8, 27, 28]. The wavelength of the computed result is in good agreement with the measurements.

7. CONCLUSIONS AND DISCUSSION

We investigated the suitability of the adjoint optimal shape design method for solving steady free-surface flows. To this end, the free-surface potential-flow problem was reformulated into an equivalent optimal-shape design problem. We then presented the adjoint optimization method for solving the design problem. We determined the asymptotic convergence behaviour of the adjoint method for sub- and supercritical flows in 2D and 3D. Moreover, we showed that preconditioning is imperative to avoid mesh-width dependence of the convergence behaviour and we presented a suitable preconditioner for the free-surface flow problem.

Numerical results were presented for two dimensional flow over an obstacle in a channel. The observed convergence behaviour is in agreement with the asymptotic estimates, i.e. the evaluation error behaves as $O(\zeta^n)$ for the supercritical test case and as $O(n^{-1/2})$ for the subcritical test case. Moreover, the numerical results confirm that the convergence behaviour of the preconditioned adjoint method is independent of the mesh width. For both test cases the computed results agree well with measurements.

The convergence behaviour of the adjoint shape optimization method for steady free-surface flows is for two dimensional problems similar to that of time-integration methods (see also Reference [8]): the error converges as $O(\zeta^n)$ for supercritical flows and as $O(n^{-1/2})$ for subcritical flows. For three dimensional problems, the anticipated convergence behaviour of the adjoint method is $O(n^{-1})$ for sub- and supercritical flows. The convergence behaviour of time-integration methods is $O(n^{-1})$ for subcritical flows and $O(\zeta^n)$ for supercritical flows. The convergence behaviour of the preconditioned adjoint method is independent of the mesh width, whereas the convergence behaviour of the usual time-integration method deteriorates with decreasing mesh width, due to a CFL-restriction on the admissible time step. Therefore, the preconditioned adjoint method is expected to be more efficient than time-integration methods, except in the case of 3D supercritical flow. However, for 3D flows and 2D subcritical flows, the convergence behaviour of the adjoint method is less efficient than the mesh-width independent $O(\zeta^n)$ convergence behaviour of the method presented in Reference [8].

The $O(n^{-1/2})$ (2D, subcritical) and $O(n^{-1})$ (3D) convergence behaviour of the adjoint method is caused by the critical modes. It is therefore anticipated that a combination of the adjoint method and a solution method that effectively eliminates the critical modes yields $O(\zeta^n)$ convergence behaviour.

ACKNOWLEDGEMENTS

This work was performed under a research contract with the Maritime Research Institute, Netherlands.

REFERENCES

1. Farmer J, Martinelli L, Jameson A. A fast multigrid method for solving the nonlinear ship wave problem with a free surface. In *Proceedings of the 6th International Conference on Numerical Ship Hydrodynamics*, Iowa, 1993.

2. Alessandrini B, Delhommeau G. Simulation of three-dimensional unsteady viscous free surface flow around a ship model. *International Journal for Numerical Methods in Fluids* 1994; **19**:321–342.
3. Campana E, Di Mascio A, Esposito PG, Lalli F. Viscous-inviscid coupling in free surface ship flows. *International Journal for Numerical Methods in Fluids* 1995; **21**:699–722.
4. Saito H, Scriven LE. Study of coating flow by the finite element method. *Journal of Computational Physics* 1981; **42**:53–76.
5. Sackinger PA, Schuck PR, Rao RR. A Newton-Raphson pseudo-solid domain mapping technique for free and moving boundary problems: A finite element implementation. *Journal of Computational Physics* 1996; **125**:83–103.
6. Tsai W, Yue DKP. Computation of nonlinear free-surface flows. *Annual Review of Fluid Mechanics* 1996; **28**:249–278.
7. Raven HC. A Solution Method for the Nonlinear Ship Wave Resistance Problem. *Ph.D. thesis*, Delft University of Technology, Netherlands, 1996.
8. van Brummelen EH, Raven HC, Koren B. Efficient numerical solution of steady free-surface Navier–Stokes flow. *Journal of Computational Physics* 2001; **174**:120–137.
9. Zhu S, Zhang Y. On nonlinear transient free-surface flows over a bottom obstruction. *Physics of Fluids* 1997; **9**(9):2598–2604.
10. Silliman WJ, Scriven LE. Separating flow near a static contact line: Slip at a wall and shape of a free surface. *Journal of Computational Physics* 1980; **34**:287–313.
11. Fursikov AV, Gunzburger MD, Hou LS. Boundary value problems and optimal boundary control for the Navier–Stokes system: the two-dimensional case. *SIAM Journal on Control and Optimization* 1998; **36**(3):852–894.
12. Becker R, Braack M, Rannacher R. Adaptive finite element methods for flow problems. *Technical Report IWR/SFB-Preprints 2000-20*, Ruprecht-Karls-Universität Heidelberg, 2000.
13. Giles MB, Pierce NA. *Adjoint Equations in CFD: Duality*, *Boundary Conditions and Solution Behaviour*. AIAA: New York, 1997; 97–1850.
14. Gunzburger MD, Kim H. Existence of an optimal solution of a shape control problem for the stationary Navier–Stokes equations. *SIAM Journal on Control and Optimization* 1998; **36**(3):895–909.
15. Gunzburger MD, Lee HK. An optimization-based domain decomposition method for the Navier–Stokes equations. *SIAM Journal of Numerical Analysis* 2000; **37**(5):1455–1480.
16. Ta'asan S. Theoretical tools for problem setup. In *Inverse Design and Optimization Methods*, van den Braembussche RA, Manna M (eds). VKI Lecture Series, vol. 5, Von Karman Institute for Fluid Dynamics, 1997.
17. Lighthill MJ. *Waves in Fluids*. Cambridge University Press: Cambridge, 1978.
18. Stoker JJ. Water Waves: the mathematical theory with applications. In *Pure and Applied Mathematics*. Courant R, Bers L, Stoker JJ (eds.) Wiley: New York, 1992.
19. Lamb H. *Hydrodynamics* (6th edn). Dover: New York, 1945.
20. Pironneau O. Optimal shape design for elliptic systems. In *Computational Physics*. Cabannes H, Holt M, Keller HB, Killeen J, Orszag SA (eds.) Springer: Berlin, 1984.
21. Whitham GB. Linear and nonlinear waves. In *Pure and Applied Mathematics*. Wiley: New York, 1974.
22. Zauderer E. Partial Differential Equations of Applied Mathematics. In *Pure and Applied Mathematics* (2nd edn), Bers L, Hilton P, Hochstadt H, Lax P, Toland J (eds.) Wiley: Chichester, 1989.
23. Ta'asan S. Multigrid one-shot methods and design strategy. In *Inverse Design and Optimization Methods*, van den Braembussche RA, Manna M (eds). VKI Lecture Series, vol. 5, Von Karman Institute for Fluid Dynamics, 1997.
24. Brandt A. Multigrid techniques: 1984 guide with applications to fluid dynamics. *Technical report*, GMD, 1984.
25. Ta'asan S. Infinite dimensional preconditioners for optimal design problems. In *Inverse Design and Optimization Methods*, van den Braembussche RA, Manna M (eds). VKI Lecture Series, vol. 5, Von Karman Institute for Fluid Dynamics, 1997.
26. Cahouet J. Etude Numérique et Experimentale du Problème Bidimensionnel de la Résistance de Vagues Non-Linéaire. *Ph.D. thesis*, ENSTA, Paris, 1984 (In French).
27. Tzabiras GD. A numerical investigation of 2D steady free surface flows. *International Journal for Numerical Methods in Fluids* 1997; **25**:567–598.
28. Vogt M. A numerical investigation of the level set method for computing free-surface waves. *Technical Report CHA/NAV/R-98/0054*, *ISSN 1101-0614*, Chalmers University of Technology, 1998.

